TURBULENT FLUX PARAMETERIZATION IN A REGIONAL-SCALE MODEL

Eberhard Müller
Deutscher Wetterdienst
Offenbach a.M., FR Germany

1. INTRODUCTION

This paper is part of the development of a limited-area regional-scale weather forecast model. The expectation that forecasts can be definitely improved by this means is based equally on higher resolution and better parameterization of physical processes. One of the prominent tasks to be attacked in this context concerns the parameterization of turbulent fluxes, especially in the atmospheric boundary layer (ABL). At this stage, a numerical resolution of the vertical ABL structure seems both necessary and useful. Necessary, because the inclusion of the diurnal cycle, topographic inhomogenity or local sources (as a result of precipitation, convection, radiation or other processes) forbids assumptions like a stationary or horizontally homogeneous state for the ABL as a whole. Useful, because the detailed time-dependent structure of the lower atmosphere has prognostic value of its own, not only for the weather itself (conditions near the ground, vertical wind shear, low level cloudiness etc.) but also for environmental applications (long-range transport of air pollution; availability of transmission parameters). In addition, the more detailed treatment of the ABL should eventually lead to a better representation of the integral properties - like dissipation of kinetic energy, cross-isobar flow and induced vertical motions, interaction between the atmosphere and the lower boundary - and their influences on the synoptic development.

It is our aim to develop a parameterization scheme for turbulent vertical fluxes which is applicable to the whole atmosphere, and to test it under the realistic conditions of a three-dimensional time-dependent meteorological model.

In conformity with the method of treatment, we divide the atmosphere into a Prandtl layer of constant flux and a remaining part, not distinguishing a priori between the Ekman layer and the free atmosphere. The theory of the Prandtl layer, which contains one information level of the model, provides us with transfer coefficients to determine the fluxes of momentum, heat, moisture, and other air properties at the lower boundary. Over land the effect of subgrid-

scale orography has been tentatively included in the roughness length. Over sea, the asymptotic case of free convection was accounted for by using the relevant scaling velocity in Charnock's formula. Regarding turbulent fluxes within the atmosphere, which is divided into non-uniform layers (normally 6 in the ABL), they are determined by gradient-flux-relations. The pertinent diffusion coefficients arise from a turbulence closure model which virtually corresponds to the level 2-type according to the hierarchy of Mellor and Yamada (1974). Specific differences refer to the procedure to define and adjust a few final parameters as well as the incorporation of a turbulent energy source not directly connected with the vertical stratification. Though such transfer and diffusion coefficients correspond to the actual atmospheric state, they are treated as uncoupled parameters generally computed at greater time intervals.

The method of testing is based on the channel version of a regional-scale meteorological model; here, processes develop under realistic but not real initial and boundary conditions. Numerical experiments comprise different models (dry, moist), initial conditions (baroclinic, barotropic), lower boundaries (sea; land with/without orography or diurnal cycle) and treatments of turbulent fluxes (Ekman type, turbulence closure model). Nevertheless, this study must confine itself to a plausibility assessment; only the verification of real forecasts will allow a final adjustment of the parameterization scheme.

2. MODELLING

2.1 The regional-scale model

At present, the regional-scale model is realized in a channel version defined on an f-plane. In the near future, the proved physical and numerical structure will be applied to a limited-area weather forecast model.

The physical structure of the moist model may be characterized by the equations of the prognostic system (see the following pages).

The formulation is based on a terrain - following σ-system between the surface and 250 mbar. The corresponding equations of the overlying p-system are easily derived by formal disposition of p^*. Most equations and quantities are self-explaining; only few remarks are appropriate.

- The prognostic equations are written and numerically realized in

The equations of the prognostic system (σ-system, moist version) I

Prognostic

$$\frac{D}{Dt}(p^*v) + p^* f k \times v = -p^*\left[\nabla\phi + RT_v \nabla \ln p^*\right] + \nabla\cdot(p^* K_M^H \nabla v) + g\frac{\partial \pi}{\partial \sigma} + p^*\left(\frac{\partial v}{\partial t}\right)_K$$

$$\frac{D}{Dt}(p^*) = 0$$

$$\frac{D}{Dt}(p^* h) = p^*\alpha\omega + p^* L_F\{S_{WE} + S_{DE} - S_{ER}\} + \nabla\cdot(p^* K_H^H \nabla h_p) + g\frac{\partial h_p}{\partial \sigma} + p^*\left(\frac{\partial h}{\partial t}\right)_K$$

$$\frac{D}{Dt}(p^* q_{DW}) = -p^*\{S_{WR} + S_{DE} + S_{WE} - S_{RD}\} + \nabla\cdot(p^* K_H^H \nabla q_{DW}) + g\frac{\partial h_{DW}}{\partial \sigma} + p^*\left(\frac{\partial q_{DW}}{\partial t}\right)_K$$

Diagnostic

$$\frac{\partial \phi}{\partial \ln p} = -RT_v \quad , \quad \alpha = \frac{1}{\rho} = \frac{RT_v}{p}$$

$$T = \frac{1}{c_p}\begin{cases} h - L_K q_{DW} \\ h - L_K Q_D(T,p) \end{cases} \qquad q_D = \begin{cases} q_{DW} \\ Q_D(T,p) \end{cases} \qquad q_W = \begin{cases} 0 & \text{unsaturated state} \\ q_{DW} - Q_D(T,p) & \text{saturation equilibrium} \end{cases}$$

$$\frac{\partial P_R}{\partial \sigma} = p^*\{S_{WR} - S_{RD} + S_{ER}\} + \left(\frac{\partial P_R}{\partial \sigma}\right)_K$$

$$\frac{\partial P_E}{\partial \sigma} = p^*\{S_{WE} + S_{DE} - S_{ER}\} + \left(\frac{\partial P_E}{\partial \sigma}\right)_K$$

The equations of the prognostic system (σ-system, moist version) II

Definitions

$$\sigma = \frac{p - p_T}{p^*} \quad , \quad p^* = p_B(x,y,t) - p_T \quad , \quad s^* = p^* \dot{\sigma}$$

$$\frac{D}{Dt}(p^*\psi) = \frac{\partial}{\partial t}(p^*\psi) + \nabla \cdot (\mathbf{v} p^* \psi) + \frac{\partial}{\partial \sigma}(s^*\psi) \quad , \quad (\ldots)_K \text{ effect of moist convection}$$

$$h = c_p T + L_K q_D \quad , \quad h_P = h + \phi$$

$$q_{DW} = q_D + q_W$$

$$T_V = \left[1 + \left(\frac{R_D}{R} - 1\right) q_D\right] T$$

$$\tau = \begin{cases} \dfrac{g\varrho^2}{p^*} K_M^V \dfrac{\partial \mathbf{v}}{\partial \sigma} & \text{atmosphere} \\ -\varrho_0 C_M \mathbf{v}_P & \text{lower boundary} \end{cases}$$

$$\{\eta_P, \eta_{DW}\} = \begin{cases} \dfrac{g\varrho^2}{p^*} K_H^V \dfrac{\partial}{\partial \sigma}\{h_P, q_{DW}\} & \text{atmosphere} \\ \varrho_0 C_H \{(h_{P,0} - h_{P,P}), (q_{DW,0} - q_{DW,P})\} & \text{lower boundary} \end{cases}$$

index 0 : level z_0 , index P : level z_P in the Prandtl layer

$P_R = \omega_R q_R$, $P_E = \omega_E q_E$ precipitation in liquid (R) or solid (E) form

flux form.

- The moist model carries information about the specific contents of water vapor (q_D) and liquid cloud water (q_W). Assuming saturation equilibrium between both phases, we have two definite prognostic equations for the specific contents of total heat (h) and water substance (q_{DW}). This is only one more than in the dry case where we used potential temperature as the thermodynamic variable. The determination of T, q_D, q_W is the object of a diagnostic procedure.

- The coefficients of subgrid-scale horizontal diffusion obey the relation

$$K_M^H = K_H^H = (k_S \Delta)^2 |\nabla v| \ ,$$

where k_S normally takes on the value 0,4. The field is recomputed every 20 time-steps (30 min) and subjected to some smoothing.

- Concerning vertical turbulent diffusion processes, the definition of the relevant parameters will be discussed below. Fluxes and gradients respectively are defined for momentum and quasiconservative quantities like dry or moist static energy, water substance or analogous pollution admixtures. At present, values needed at level z_o are prescribed; for real data simulations a soil model is being developped.

- Stable precipitation is supposed to be in equilibrium with the meteorological conditions of a vertical air column (stationary and horizontally homogeneous state). Conversion rates (S) between water vapor (D), cloud water (W), rain (R), and snow (E) are taken into account, L_K (L_F) means latent heat of condensation (freezing).

- Convective processes are considered to be adequately treated by turbulence parameterization in the dry case. For the moist model, an additional scheme of penetrating moist convection is being tested but has not been included in the experiments quoted.

- So far, radiation effects have not been taken into account.

- Horizontal diffusion of vertically averaged divergence in the upper p-system has proved to be an effective and meteorologically harmless means to dampen the first vertical modes of inertial gravity waves.

The finite difference form of the model equations is based upon the grid structure laid out in Fig. 1. Vertically, the atmosphere is

VERTICAL

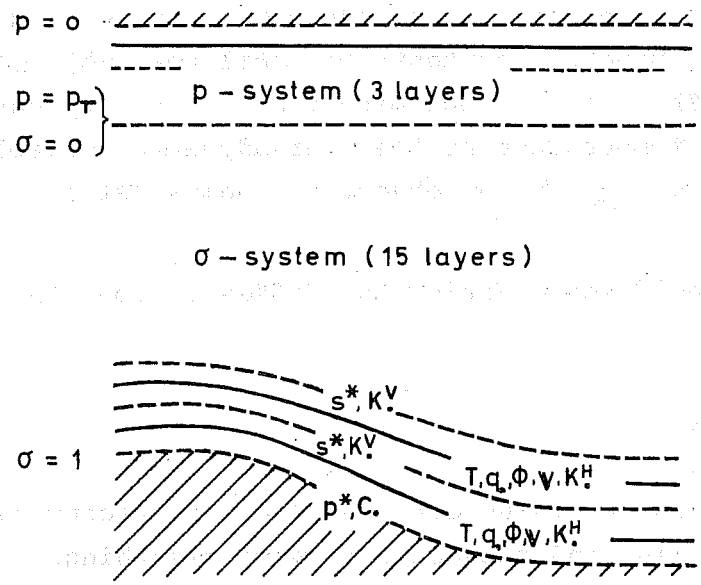

K	p [mb] / σ	p_M [mb]	z_M [m]
1	50.0		20500
2	137.5		14000
3	212.5		11300
4	0.050	288	9300
5	0.150	363	7800
6	0.250	438	6500
7	0.350	513	5300
8	0.450	588	4300
9	0.550	663	3350
10	0.635	726	2600
11	0.705	779	2060
12	0.770	828	1570
13	0.825	869	1170
14	0.875	906	820
15	0.920	940	520
16	0.955	966	290
17	0.980	985	130
18	0.995	996	30

HORIZONTAL

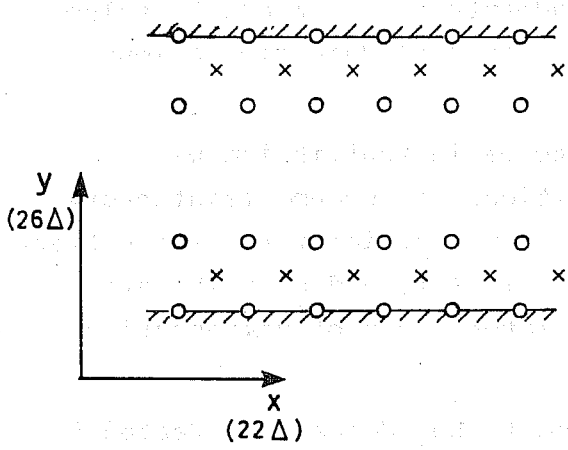

Disposition of variables
(even time level)

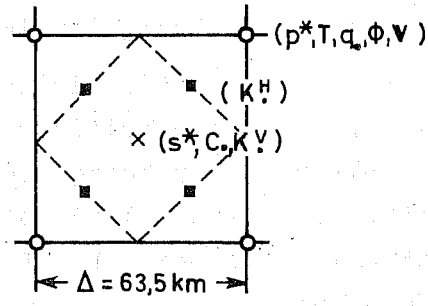

TEMPORAL

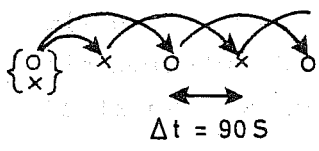

Fig. 1 Grid structure of the regional-scale model (channel version)

divided into layers of upward increasing thickness. The minimum number of necessary layers in the ABL region was decided experimentally. At the center of mass of the layers, all prognostic variables (plus geopotential) are defined and horizontal fluxes as well as local effects of some parameterized processes are calculated. At levels separating different layers, all vertical fluxes are determined. Horizontally, the grid is staggered in time (even and odd time levels). As a consequence, divergences of horizontal fluxes and gradients can be defined over one grid interval (63,5 km), thus nearly doubling the effective resolution. In order to achieve compactness and to keep time levels together, horizontal diffusion terms are evaluated by means of a 5-point operator needing K_M^H (K_H^H)-values half-way between corner and center grid-points. Time integration is accomplished by an explicit leapfrog procedure (time step: 90 s). Nevertheless, in the numerical formulation implicit components arise from Coriolis terms, horizontal diffusion (Dufort-Frankel scheme), vertical diffusion (Crank-Nicolson scheme), and vertical transport terms. The resulting system of linear equations for each variable (complex treatment of horizontal velocity), characterized by a tridiagonal matrix, is solved non-iteratively by the Gauß elimination method.

The dimensions of the channel are 1397 km (22Δ) in length and 1651 km (26Δ) in width. Concerning the lateral boundaries, we assume periodicity in x and rigid, smooth, isolating walls in y. The upper boundary is closed, at the lower boundary diffusive fluxes are taken into account.

2.2 The parameterization of turbulent fluxes

2.2.1 Fluxes at the lower boundary

For a model of this type, it is a rather obvious procedure to introduce a constant flux (or Prandtl) layer adjacent to the ground and to apply the well-established results of the similarity theory. Using the Dyer-Businger relations (Businger, 1973) in their integrated form modified by Louis (1977, 1979), we have the following formulas for the transfer coefficients which appear in the prognostic equations (see 2.1):

$$C_M = \begin{cases} \gamma |v_p| \left(1 - \frac{b}{2} \frac{x}{v_p^2}\right)^2, & \text{for } x \geq 0 \\ & \left(\frac{x}{v_p^2} \leq \frac{2}{b}\right) \\ \gamma \left(|v_p| - \dfrac{bx}{|v_p| + \gamma b a_M \left(\frac{\Phi_p}{\Phi_0}\right)^{\frac{1}{2}} |x|^{\frac{1}{2}}}\right), & \text{for } x \leq 0 \end{cases} \qquad (1)$$

$$C_H = \begin{cases} \frac{1}{d}\gamma|v_P|\left(1-\frac{b}{2}\frac{x}{v_P^2}\right)^2, & \text{for } x \geq 0 \\ & \left(\frac{x}{v_P^2} \leq \frac{2}{b}\right) \\ \frac{1}{d}\gamma\left(|v_P| - \frac{bx}{|v_P| + \gamma b a_H \left(\frac{\phi_P}{\phi_0}\right)^{\frac{1}{2}} |x|^{\frac{1}{2}}}\right), & \text{for } x \leq 0 \end{cases} \qquad (2)$$

The definitions of functions and parameters are

$$x = \phi_P \frac{\Theta_P - \Theta_0}{\Theta_0} \; , \quad \gamma = \left(\frac{k_T}{\ln \frac{\phi_P}{\phi_0}}\right)^2 , \quad \phi = gz \; ;$$

$a_M = 7.4$, $a_H = 5.3$, $b = 9.4$, $d = 0.74$, $k_T = 0.35$.

Index P marks an appropriate level within the Prandtl layer (our lowest level), index 0 refers to level z_0. The special case of free convection ($|v_P| \approx 0$, $x < 0$) is covered by this parameterization, implying

$$\frac{C_H}{C_M} = \frac{a_M}{a_H}\frac{1}{d} = 1.89;$$

the stable branch retains the neutral value of $1/d = 1.35$.

For gridpoints over land, z_0 has to be prescribed and formulas (1), (2) have an explicit character. One may combine the effects of land use (z_{oB}) and subgrid-scale orography (z_{oR}) on the roughness length:

$$z_o = z_{oB} + z_{oR} \qquad (3)$$

z_{oB} is set equal to 15 cm in the relevant experiments. z_{oR} has been estimated using a modified form of Kutzbach's formula (WMO, 1973):

$$z_{oR} = 0.8 \frac{h_S^2}{L_R} \qquad (4)$$

L_R means a typical distance between mountains (set to 40 km). Concerning h_S (RMS of subgrid-scale orography), we arrived at a good linear regression on the gridscale (model) height (z_B)

$$h_S = 23\ 68 + 0.1842\ z_B \ [\text{cm}] \qquad (5)$$

for the region of the Alps on the basis of the USAF/NCAR data. Consequently, in experiments including model Alps z_0 varies between 16.1 and 3520 cm.

For gridpoints over sea, relations (1), (2) are no longer explicit if Charnock's formula

$$\Phi_0 = \alpha_0 u_*^2 \; (= \alpha_0 C_M |v_p|) \; , \; \alpha_0 = 0.032 \tag{6}$$

is applied. In the limiting case of free convection, we use

$$u_+ = \left(\frac{\Phi_p \eta_0}{\Theta_0 \varrho_0} \right)^{\frac{1}{3}} , \qquad \Phi_p \eta_0 \quad \text{surface heat flux} \tag{7}$$

as scaling velocity and venture the interpolation

$$\Phi_0 = \alpha_0 \left(u_*^2 + u_+^2 \right) \tag{8}$$

on the unstable side.

2.2.2 Fluxes within the atmosphere

With regard to the parameterization of turbulent fluxes above the Prandtl layer, one cannot fall back upon ready-made solutions. Instead of proceeding in a totally heuristic manner, we shall base our considerations on the equations of second turbulent moments. As shown by Mellor and Yamada (1974), even a purely diagnostic treatment (their Level 2) is able to reproduce the essential aspects of more complex versions. In a somewhat independent way such a diagnostic system was derived and matched with the Prandtl layer parameterization.

Considering a dry atmosphere we start from the well-known prognostic equations for the components of stress tensor (deviator), potential temperature flux vector, and for the turbulent kinetic energy and potential temperature variance. After neglecting Coriolis terms and molecular effects except for the dissipation of quadratic quantities, we make the system diagnostic in character by the assumption of local equilibrium. The next step refers to parameterizations of the pressure fluctuation correlation and dissipation terms. Assuming horizontal homogeneity of the mean fields, we arrive after some algebraic manipulation at the following equations:

$$\tau \equiv -\frac{\tau}{\varrho} = \frac{\dfrac{\delta}{C_M e_T^{\frac{1}{2}}} \left[\dfrac{2}{3} \alpha e_T \dfrac{\frac{1}{C_S^2} \delta^2 \frac{2}{3} \beta \frac{g}{\Theta} \frac{\partial \Theta}{\partial z}}{1 + 2 \frac{\gamma}{C_0} \frac{1}{C_S} \frac{\delta^2}{e_T} \frac{g}{\Theta} \frac{\partial \Theta}{\partial z}} \right]}{1 + \dfrac{1}{C_M C_S} \dfrac{\delta^2}{e_T} \dfrac{g}{\Theta} \dfrac{\partial \Theta}{\partial z}} \; \frac{\partial v}{\partial z} \tag{9}$$

$$\gamma_z \equiv \frac{\eta_p}{\varrho c_p} = - \frac{\frac{\delta}{C_S e_T^{\frac{1}{2}}} \left[\frac{2}{3} \beta e_T \right]}{1 + 2 \frac{\gamma}{C_\Theta} \frac{1}{C_S} \frac{\delta^2}{e_T} \frac{g}{\Theta} \frac{\partial \Theta}{\partial z}} \frac{\partial \Theta}{\partial z} \tag{10}$$

$$e_T = \frac{\delta}{C_\varepsilon e_T^{\frac{1}{2}}} \left[\ell \cdot \frac{\partial v}{\partial z} + \frac{g}{\Theta} \gamma_z \right] \tag{11}$$

for the vertical fluxes of momentum (τ) and heat (η_p), needed in the prognostic system, as well as turbulent kinetic energy (e_T). Avoiding the assumption of equipartitioned turbulent energy used here does not change the mathematical structure but only some parameter combinations.

Obviously, Eqs. (9), (10) represent flux-gradient relations which give the possibility to determine diffusion coefficients. Algebraic transformations lead to the following practical procedure. Knowing the gradient Richardson number

$$Ri = \frac{\frac{g}{\Theta} \frac{\partial \Theta}{\partial z}}{\left(\frac{\partial v}{\partial z} \right)^2} , \tag{12}$$

we can determine the flux Richardson number

$$Rf = \frac{- \frac{g}{\Theta} \gamma_z}{\ell \cdot \frac{\partial v}{\partial z}} \tag{13}$$

by means of a quadratic equation

$$Rf = c_1 \left[Ri + c_2 - \left(Ri^2 - c_3 Ri + c_2^2 \right)^{\frac{1}{2}} \right] . \tag{14}$$

It proves convenient to define a new stability parameter

$$\Gamma = \frac{Rf}{1 - Rf} \tag{15}$$

which takes on the values -1, 0, $\Gamma^{(\kappa)}$ for the cases of free convection, neutral stratification, and critical stability respectively. By means of the stability functions

$$G(\Gamma) = \frac{1 - b_1 \Gamma}{1 - b_2 \Gamma} \qquad \text{and} \tag{16}$$

$$S_M(\Gamma) = \frac{1 - a \Gamma}{G(\Gamma)} , \tag{17}$$

we are finally able to determine the turbulent Stanton number

$$\alpha_H \equiv \frac{K_H^v}{K_M^v} = \alpha_H^{(N)} G \ , \tag{18}$$

where $\alpha_H^{(N)}$ means its value in the neutral case, and the diffusion coefficient for momentum:

$$K_M^v = (k_T \delta)^2 S_M^{\frac{3}{2}} \left[\left(\frac{\partial v}{\partial z} \right)^2 - \alpha_H \frac{g}{\Theta} \frac{\partial \Theta}{\partial z} \right]^{\frac{1}{2}} \tag{19}$$

Eqs. (9)-(11) contain 7 parameters - $C_M, C_S, C_E, C_\Theta, \alpha, \beta, \gamma$ - which arise from the parameterization relations. Parameters of this primary type are difficult to determine (cf. Deardorff, 1973, or Mellor, 1973). On the other hand, one can show that the parameters appearing in the system of equations (14)-(19) - a, b_1, b_2, c_1, c_2, c_3, k_T - are fixed by only 4 conditions. For this purpose, we chose common and well-discussed quantities or relations which can be adapted easily to the current state of knowledge. To increase the number of degrees of freedom, stable and unstable branches, which overlap in the neutral state, are adjusted separately. The conditions are in the neutral case

$$K_M^v = (k_T \delta)^2 \left| \frac{\partial v}{\partial z} \right| \tag{20a}$$

$$\alpha_H = \frac{1}{d} = 1.35 \ , \tag{20b}$$

in the case of critical stability

$$\alpha_H = 1 \tag{21a}$$

$$Ri = \frac{2}{b} = 0.21 \ , \tag{21b}$$

in the case of free convection

$$K_H^v = (k_T \delta)^2 C_K^{\frac{3}{2}} \left(-\frac{g}{\Theta} \frac{\partial \Theta}{\partial z} \right)^{\frac{1}{2}} , \quad C_K = 5.03 \tag{22a}$$

$$\alpha_H = 2.57 \ . \tag{22b}$$

The constant C_K is connected with the "universal" constant C_1 of Monin and Yaglom (1971) by the relation

$$C_K = \frac{3}{C_1 (k_T)^{\frac{4}{3}}} \tag{23}$$

according to which C_K should lie within the interval $3.4 \ldots C_K \ldots 5.3$. To be consistent with the Prandtl layer parameterization, all parameters agree with the Dyer-Businger relations (Businger, 1973), though there is some doubt about their correctness (Wieringa, 1980). The constants in (22a,b) were derived from these relations (showing a different asymptotic behavior) within their range of validity ($-2.5 \leq \zeta = \frac{z}{L} \leq 0$) by the least square method using the following analogies

$$\frac{K_M^V}{(k_T \delta)^2 \left|\frac{\partial v}{\partial z}\right|} = \boxed{S_M^{\frac{3}{2}} (1 - \alpha_H Ri)^{\frac{1}{2}} \triangleq \frac{1}{\phi_M^2 (\zeta(Ri))}} = \frac{K_M^V}{(kz)^2 \left|\frac{\partial v}{\partial z}\right|} \tag{24a}$$

$$\alpha_H = \boxed{\alpha_H^{(N)} G \qquad \triangleq \frac{\phi_M (\zeta(Ri))}{\phi_H (\zeta(Ri))}} . \tag{24b}$$

The characteristic length δ is assumed to be dependent on height according to Blackadar's (1962) formula

$$\delta = \frac{z}{1 + \frac{z}{\delta_\infty}} , \qquad \delta_\infty = 100 \text{ m or } 500 \text{ m} \tag{25}$$

At the moment δ_∞, which is related to the standard asymptotic mixing length ℓ_∞ by $\ell_\infty = k_T \delta_\infty$, is considered to be a prescribed parameter independent of the atmospheric state (in contrast to some other authors, e.g. Mellor and Yamada, 1974).

The parameterization scheme described above, exhibits the known strong dependence on stability, resulting in K_M^V, K_H^V being zero over greater portions of the model atmosphere. It was felt that a source of turbulent energy representing the horizontal structure of meteorological processes should be incorporated - not only for numerical reasons. We chose the dissipation rate due to horizontal diffusion

$$\varepsilon_S = \frac{1}{(k_S \Delta)^4} (K_M^H)^3 \tag{26}$$

assuming energy cascading into the turbulence range. The modified form of Eq. (11) is

$$e_T = \frac{\delta}{C_E e_T^{\frac{1}{2}}} \left[\mathbb{t} \cdot \frac{\partial v}{\partial z} + \frac{g}{\Theta} b_z + \varepsilon_S \right] \tag{27}$$

Using

$$Rg = \frac{-\frac{g}{\Theta} b_z}{\mathbb{t} \cdot \frac{\partial v}{\partial z} + \varepsilon_S} = \alpha_H \frac{\frac{g}{\Theta} \frac{\partial \Theta}{\partial z}}{\left(\frac{\partial v}{\partial z}\right)^2 + \frac{\varepsilon_S}{K_M^v}} \tag{28}$$

instead of Rf and defining

$$\Gamma = \frac{Rg}{1 - Rg} \,, \tag{29}$$

one can show that the functions $G(\Gamma), S_M(\Gamma), \alpha_H(\Gamma)$ remain unchanged. According to the right-hand part of Eq. (28), Rg is always subcritical for $\varepsilon_S > 0$. Conformably, the stability dependence in the Prandtl layer formulation (1), (2) has been relaxed by the modification $\left(1 - \frac{b}{2} \frac{x}{v_p^2}\right)^2 \Rightarrow e^{-b \frac{x}{v_p^2}}$ (cf. Tiedtke et al., 1979). The computation of K_M^v, K_H^v is now based on

$$\left(K_M^v\right)^3 - K_M^v \left(k_T \delta\right)^4 \left(\frac{\partial v}{\partial z}\right)^2 - \left(k_T \delta\right)^4 \varepsilon_S = 0 \tag{30a}$$

$$K_H^v = \alpha_H^{(N)} K_M^v \tag{30b}$$

in the neutral case and

$$K_M^v = \left(k_T \delta\right)^2 S_M^{\frac{3}{2}} \left[\frac{\alpha_H}{\Gamma} \frac{g}{\Theta} \frac{\partial \Theta}{\partial z} \right]^{\frac{1}{2}} \tag{31a}$$

$$K_H^v = \alpha_H K_M^v \tag{31b}$$

in all other cases. Γ follows from an implicit equation:

$$\frac{\Gamma \varepsilon_S}{\alpha_H(\Gamma) \frac{g}{\Theta} \frac{\partial \Theta}{\partial z} - \Gamma \left[\left(\frac{\partial v}{\partial z}\right)^2 - \alpha_H(\Gamma) \frac{g}{\Theta} \frac{\partial \Theta}{\partial z} \right]} = \left(k_T \delta\right)^2 S_M^{\frac{3}{2}}(\Gamma) \left[\frac{\alpha_H(\Gamma)}{\Gamma} \frac{g}{\Theta} \frac{\partial \Theta}{\partial z} \right]^{\frac{1}{2}} \tag{32}$$

which is applied in various forms according to stability ranges. It turned out that one iteration is sufficient if the previous values of K_M^v, K_H^v are used as a first guess. New values are determined every 20 time steps (30 min), slight temporal smoothing being appropriate in the lowest levels. The turbulent flux part of the model requires about 5 % of the whole computational effort.

The inclusion of saturated moist turbulent processes (within clouds) may be handled in an analogous manner. The measures of thermal stability written for the dry or unsaturated case in a new form

$$N^2 \equiv \frac{g}{\Theta}\frac{\partial \Theta}{\partial z} = \frac{1}{c_p T}\frac{\partial \phi}{\partial z}\frac{\partial}{\partial z}(c_p T + \phi) \tag{33}$$

$$\times \equiv \frac{\phi_p}{\Theta_o}(\Theta_p - \Theta_o) = \frac{1}{c_p T_o}\left[\phi\right]_o^p \left[c_p T + \phi\right]_o^p \tag{34}$$

have to be replaced by

$$N^2 = \frac{1}{c_p T}\frac{\partial}{\partial z}(\phi + L_k Q_D)\frac{\partial}{\partial z}(c_p T + \phi + L_k Q_D) \tag{33'}$$

$$\times = \left[\phi + L_k Q_D\right]_o^p \left[c_p T + \phi + L_k Q_D\right]_o^p . \tag{34'}$$

Until now, turbulent energy production has been restricted to dry sources in the moist model as well. In the presence of an adequately parameterized convection, that should not be the case any longer.

3. PHENOMENA IN NUMERICAL EXPERIMENTS RELATED TO TURBULENT PROCESSES

In the course of model development, some experiments (Table 1) are directly related to significance and parametric formulation of turbulent fluxes. Selected results have been assembled under meteorological aspects. These examples should illustrate the performance of the parameterization scheme used in the context of 3-dimensional regional-scale processes and allow plausibility assessments. This contrasts with 1-dimensional simulations which are usually verified against Wangara data (cf. Mellor and Yamada, 1974; Yamada and Mellor, 1975; Yamada, 1977).

3.1 The atmosphere as a whole

In all experiments related to baroclinic development, we find two regions essentially affected by turbulent processes: the ABL and the layer of maximum wind (LMW). This is reflected not only in maximum rates of energy dissipation (demonstrable but not shown here; cf. Chen, 1974) but also in the cross-isobar angle (Fig. 2) and dimensionless numbers characterizing the relative importance of the ageo-

Table 1 Information about numerical experiments related to boundary layer aspects

Designation of experiment	B16	B18	B19	B20	B21	B22	B24D	B25D	B28	B27D	C16A	C17
Purpose of experiment	dry baroclinic development				diurnal cycle	land-sea contrast		lee cyclogenesis orographic effects		orographic effect on barotropic flow	moist baroclinic development	diurnal cycle
Model type	dry version										moist version with hydrological cycle	
Initial state: Mass field	dry baroclinic									dry barotr.	weakly moist baroclinic	
Initial state: Stat. stab.	weakly dry stable									standard	weakly moist stable	
Initial state: Dis-turbance	p*							orography cut out			p*	
Initial state: Wind	geostrophic											
Treatment of turbulent fluxes	$K_M^V=10\frac{m^2}{s}$ $K_H^V=0$	complete parameterization scheme providing C_M, C_H, K_M^V, K_H^V										
		δ_∞=100m, ε_s not included						δ_∞ = 500 m, ε_s included				
Boundary layer resolution	5 layers below $\sigma=0.5$	10 layers below $\sigma=0.5$, thickness decreasing downwards										
Earth's surface	v=0	sea		land	diurnal cycle of temp.	land/sea half and half	land	land with orography	orograph. roughness		land	diurnal cycle of temp.

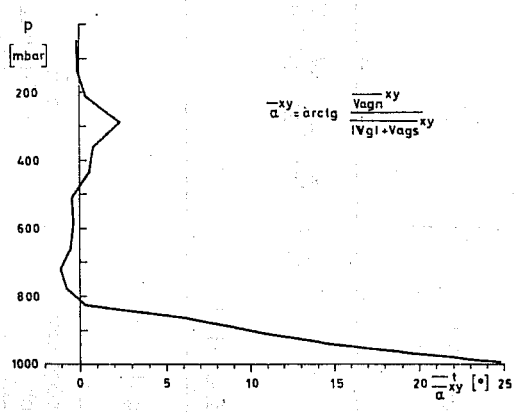

Fig. 2

Cross-isobar angle averaged horizontally and over the time interval 42 - 60 h (Exp. B24D)

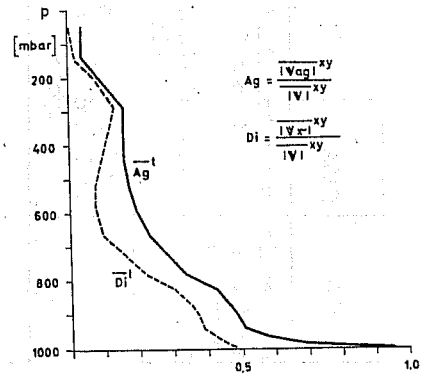

Fig. 3

Dimensionless numbers characterizing the relative importance of the ageostrophic (Ag) and divergent (Di) part of the wind vector (Exp. B24D; averaged over the time interval 42 - 60 h)

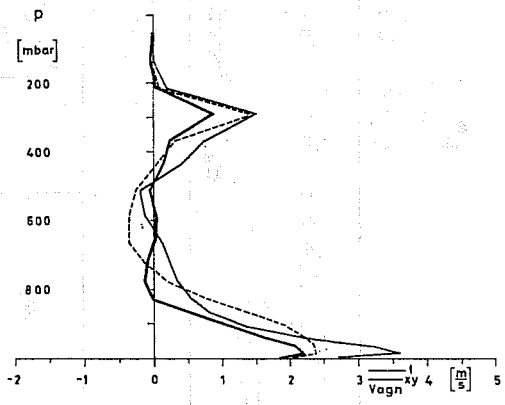

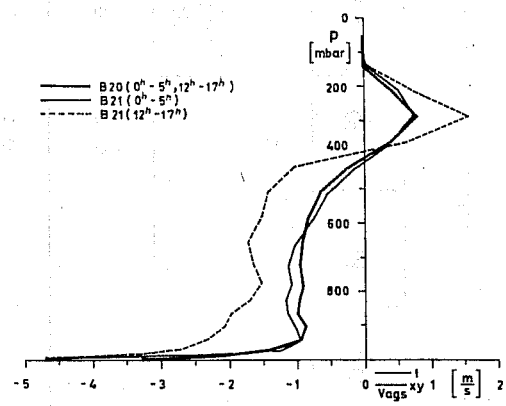

Fig. 4a

Fig. 4b

Ageostrophic wind components normal (a) and parallel (b) to the geostrophic wind vector, averaged horizontally and over simulated time intervals of day including two diurnal cycles each (Exp. B21; Exp. B20 for comparison)

strophic and divergent parts of the wind vector (Fig. 3). As for the ageostrophic wind component normal (v_{agn}, Fig. 4a) and parallel (v_{ags}, Fig. 4b) to the geostrophic wind vector, the general vertical structure is clear: $v_{agn} > 0$ in ABL and LMW, $v_{ags} < 0$ in ABL and $v_{ags} > 0$ in LMW. The diurnal cycle seems to have definite effects even on LMW. Here v_{agn} is generally increased compared to the experiment with fixed surface temperature; in the ABL region we find the expected differences between day and night, nearly canceled in the vertical integral. Outstanding is the day-time profile of v_{ags}.

3.2 The boundary layer within the synoptic system

A fully developped dry cyclone (Fig. 5) displays a typical horizontal distribution of turbulent diffusion (Fig. 6). The thermal stratification causes small (large) values of K_M^v in the front (rear) part of the cyclone, whereas wind speed is responsible for a minimum near the circulation center and an annulus of large values around it. In the vertical (Fig. 7a), a maximum of K_M^v at some height between 200 m (high pressure region) and 650 m (bursts of cold air) as well as minimum values at the ABL boundary are noticeable. Especially impressive is such a cross-section of a cyclone passing over a mountain range (Fig. 7b). The influence of surface conditions may be demonstrated by the cross-isobar angle of the Prandtl layer flow (Fig. 8). Values over sea (15^o-20^o) contrast with those over land (25^o-30^o), varying between 20^o (day) and 40^o (night) within the diurnal cycle. One has to consider an adaptation time of about 36 h if starting from geostrophic conditions. In the whole course of baroclinic development, the vertical profile of turbulent heat flux (Fig. 9) is characterized by (large) positive values in the (lower) ABL and small negative values above including a relative maximum near its upper boundary. The overall effects of ABL features on the baroclinic development may be assessed by the horizontal variation of surface pressure (Table 2). Significant differences obviously exist between Ekman-type and second order parameterization of the ABL (B16-B18,19) as well as between land and sea surface (B20-B19), the land/sea case (B22) lying exactly in the middle. Small effects seem to arise from increasing δ_∞ (B18 → B19), including ϵ_S (B20 → B24D) or accounting for subgrid-scale orographic roughness (B25D → B28). Surprisingly, the diurnal cycle (B21) brings the land case (B20) close to the sea case (B19).

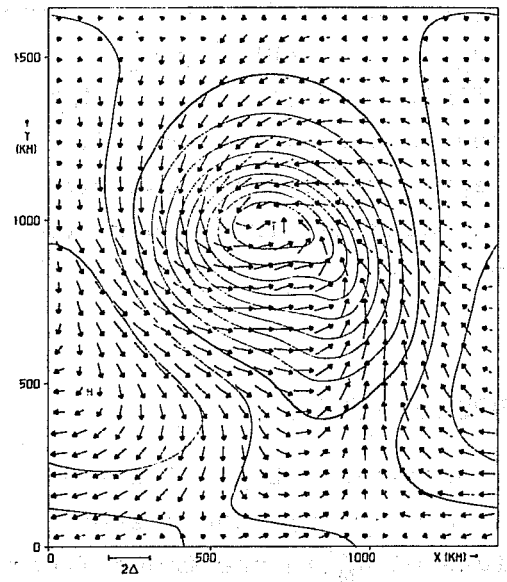

Fig. 5

Surface pressure (mbar) and flow field at level σ = 0.995 (Exp. B24D, time 57 h)

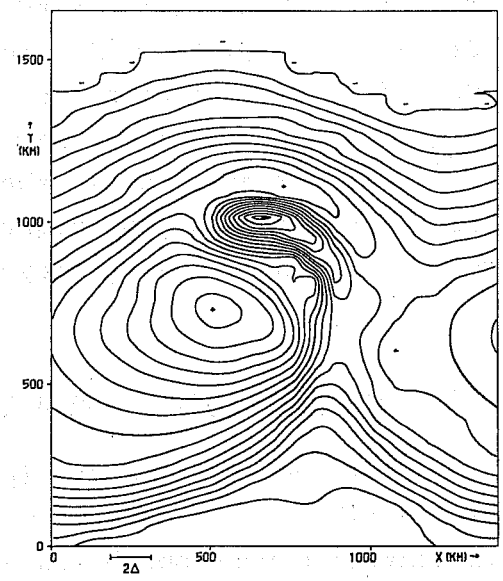

Fig. 6

Coefficient of turbulent diffusion ($m^2\ s^{-1}$) at level σ = 0.99 (Exp. B24D, time 57 h)

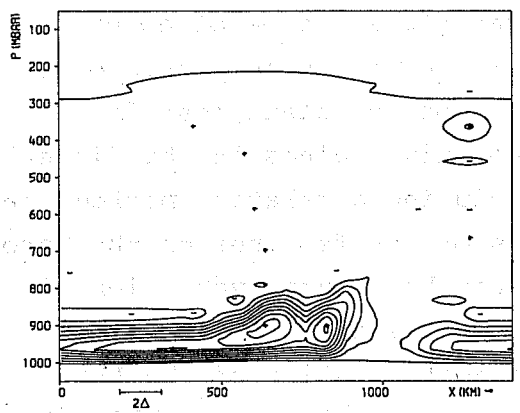

Fig. 7a

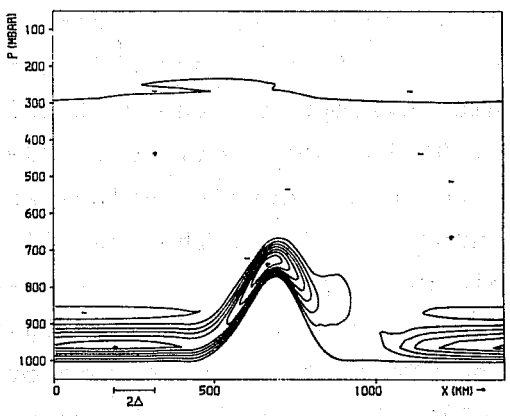

Fig. 7b

Coefficient of turbulent diffusion (10 $m^2\ s^{-1}$) in a (x,z)-cross-section through the center of the channel for Exp. B24D, 57 h (a) and Exp. B28, 58 h (b)

Table 2 Difference in surface pressure (mbar) between high and low center for different experiments and forecast lengths

EXPERIMENT	00 h	12 h	24 h	36 h	48 h	60 h	72 h
B16	3.00	3.14	4.45	6.29	7.69	8.68	9.36
B18	3.00	4.11	7.96	12.12	14.37	15.68	15.45
B19	3.00	4.11	7.93	11.97	14.21	15.30	14.94
B20	3.00	3.82	6.91	9.84	11.24	12.01	11.81
B21	3.00	3.91	7.25	11.12	14.23	15.04	15.68
B22	3.00	4.00	7.57	10.84	12.35	13.61	13.38
B24D	3.00	3.82	7.00	9.96	11.26	12.02	11.97
B25D	0.00	0.93	1.81	3.19	5.14	6.44	9.78
B28	0.00	1.00	2.03	3.48	5.42	6.98	10.03

3.3 Diurnal cycle

The diurnal cycle has been realized by an oscillating surface temperature corresponding to undisturbed days in May over central Europe; specific humidity is held fixed in moist experiments. The valve function of the ABL is clearly demonstrated for heat (Fig. 10) and stack emitted sulphur dioxide (Fig. 11). The temporal variations of frictional forces result in a time-height dependency of the cross-isobar angle in the ABL region (Fig. 12). Under conditions of strong stability and weak meteorological development (moist experiments), this picture proves to be rather complicated (Fig. 13), involving pronounced inertial oscillations which are best illustrated by hodographs. Compared to the background experiment (Fig. 14a) which exhibits damped inertial oscillations until 36 h at the 290 m-level, the experiment with diurnal cycle included (Fig. 14b) shows the following sequence of events: 0^h-9^h movement on inertial circle, 9^h-11^h rapid adjustment with little further change in the day-time, 19^h-10^h movement on another inertial circle. Under this aspect the analysis at 12 GMT should favour initialization over Europe. Even if the energy dissipation is remarkably increased by the diurnal cycle (Fig. 15; maximum in the day-time) this effect is overcompensated by the conversion of enthalpy into kinetic energy (Fig. 16; maximum at night) confirming our earlier statement about the overall effect.

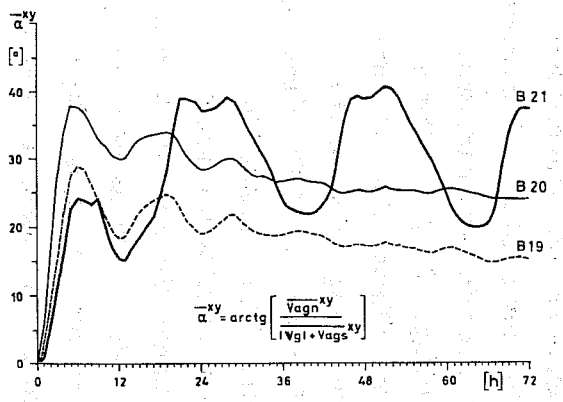

Fig. 8 Cross-isobar angle (horizontal average) at level $\sigma = 0.995$ over sea (Exp. B19), land (Exp. B20), land exhibiting diurnal cycle of temperature (Exp. B21)

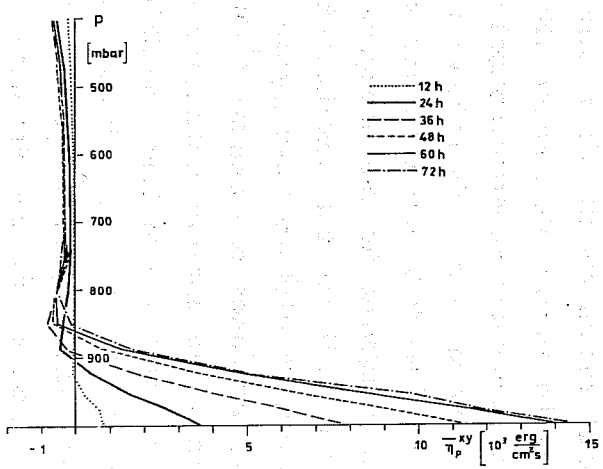

Fig. 9 Turbulent heat flux (horizontal average) for proceeding Exp. B24D

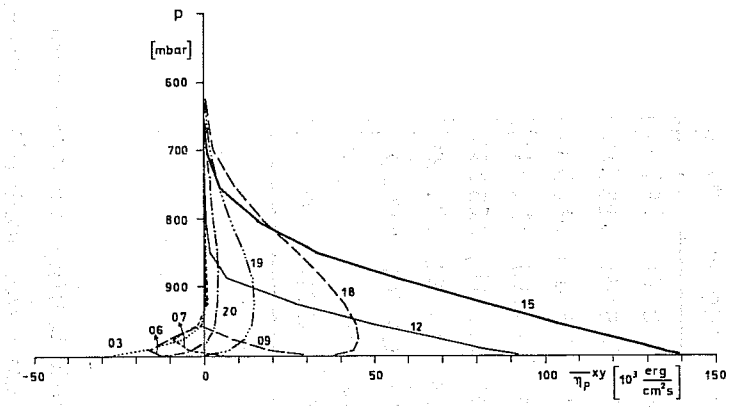

Fig. 10 Turbulent heat flux (horizontal average) during the diurnal cycle (Exp. B21, time 33 h (09 h) - 55 h (07 h))

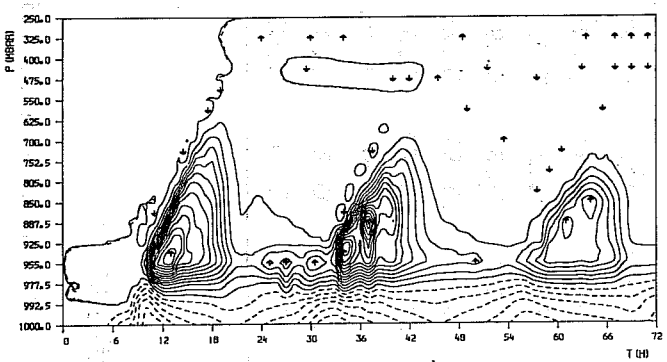

Fig. 11 Turbulent flux of sulphur dioxide (0.3 pg cm^{-2} s^{-1}; horizontal average) for Exp. B24-KA9 simulating long-range transmission of sulphur compounds under the influence of a diurnal cycle

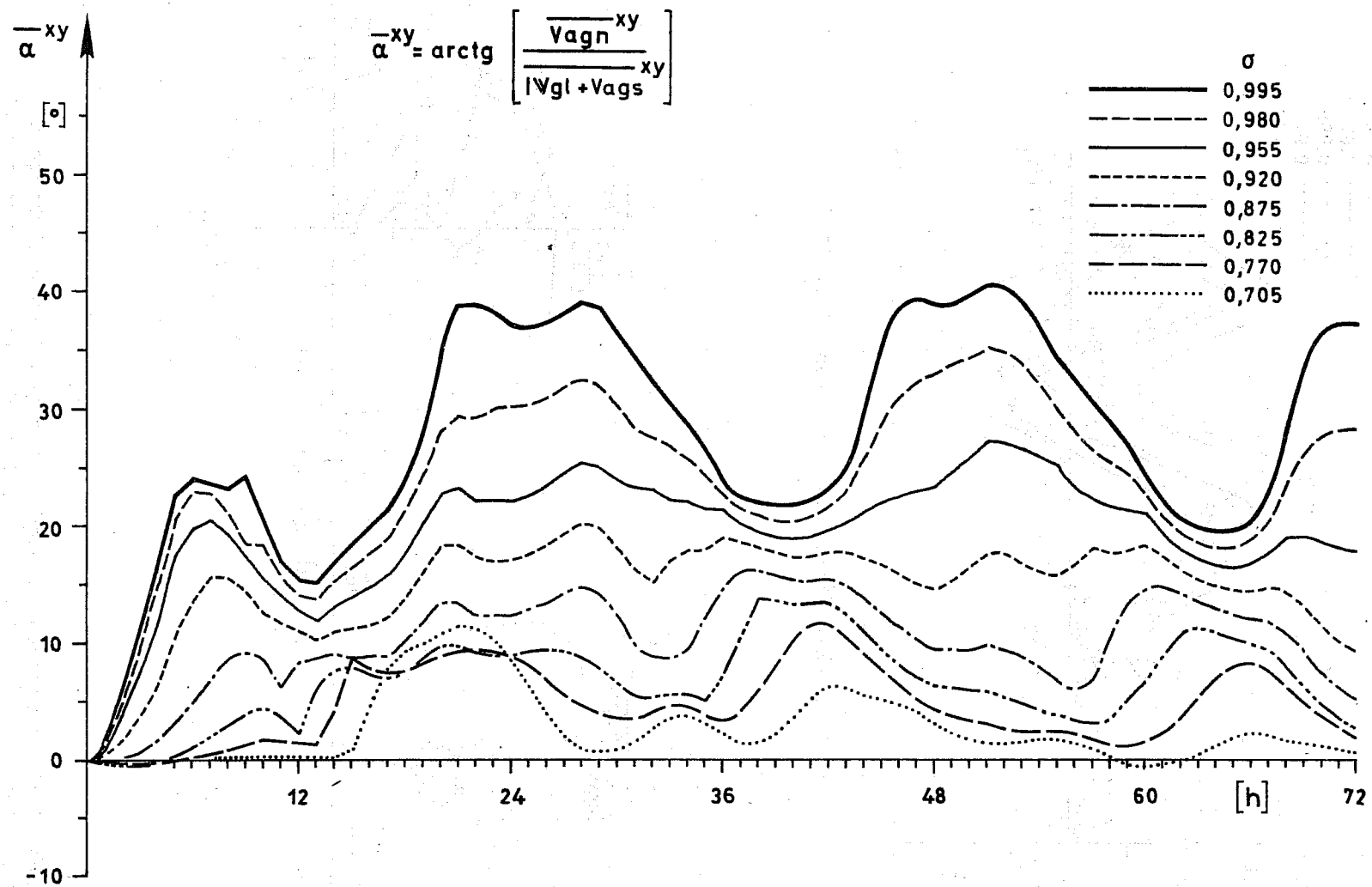

Fig. 12 Cross-isobar angle (horizontal average, Exp. B21)

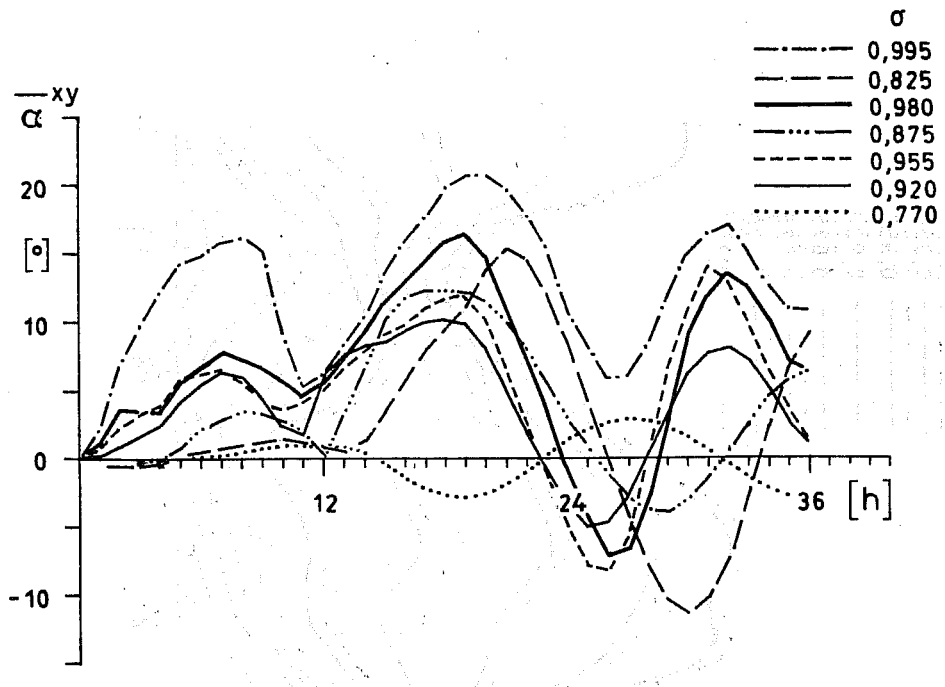

Fig. 13 Cross-isobar angle (horizontal average, Exp. C17)

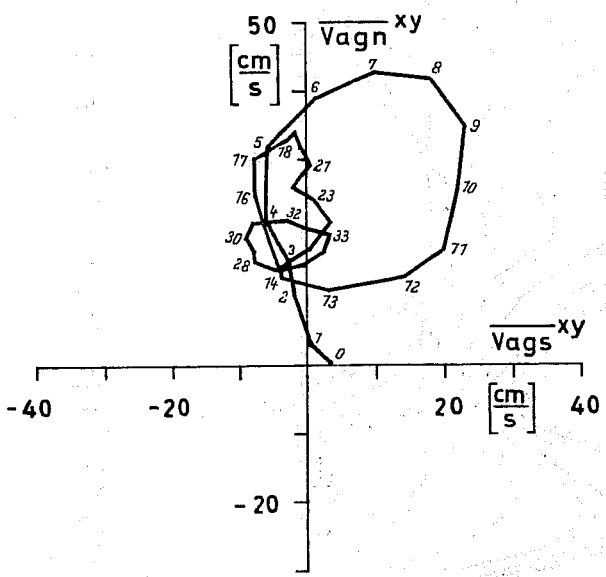

Fig. 14a

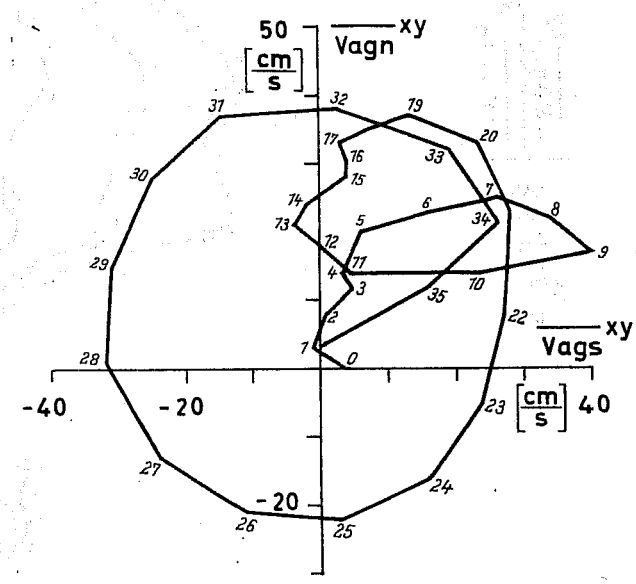

Fig. 14b

Hodographs of the ageostrophic wind vector (horizontal average at level $\sigma = 0.955$ for Exp. C16A (a) and Exp. C17 (b). Numbers signify time in hours.

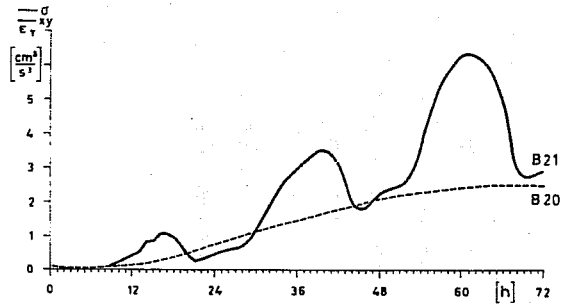

Fig. 15 Mean tropospheric rate of dissipation of kinetic energy by turbulent processes for experiments with (Exp. B21) and without (Exp. B20) diurnal cycle

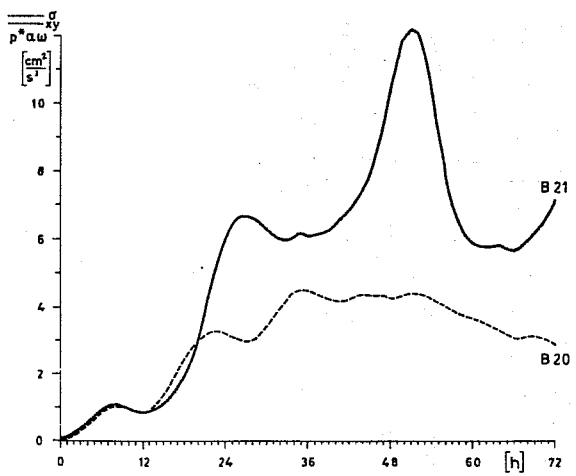

Fig. 16 Mean tropospheric rate of conversion from enthalpy into kinetic energy for experiments with (Exp. B21) and without (Exp. B20) diurnal cycle

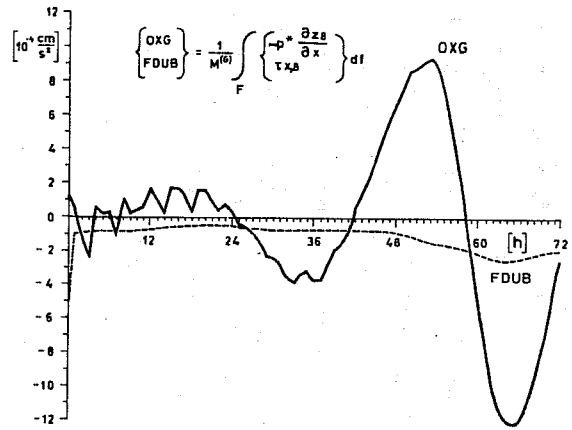

Fig. 17a

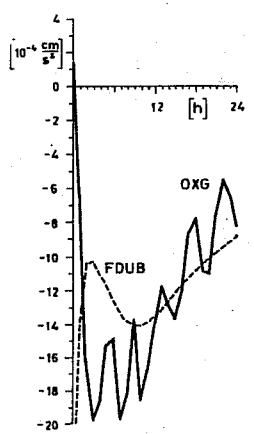

Fig. 17b

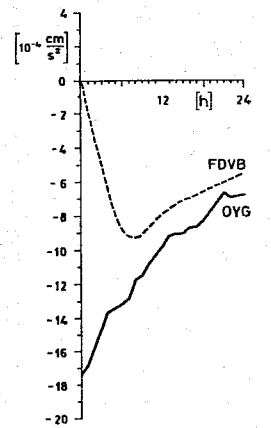

Fig. 17c

Rate of change of mean atmospheric (x,y)-momentum as a result of pressure drag by mountains (OXG,OYG) and surface friction (FDUB, FDVB) a) Lee cyclogenesis and further baroclinic development (Exp. B28)
b,c) Barotropic flow (Exp. B27D)

3.4 Surface friction as compared to orographic pressure drag

Mountain effects have been simulated in the channel by putting the typical arc of the Alps into a central position with an orientation normal to the basic current (U). Under baroclinic initial conditions (U increases upwards from 0 to 50 $\frac{m}{s}$ in the tropospheric frontal zone; mountains are cut out from the mass field), a lee cyclone develops; it begins to migrate after 26 h and passes over the Alps around 58 h. Contrary to surface friction (FDUB), orographic pressure drag (OXG) effects (Fig. 17a) are highly time-dependent corresponding to the changing position of the low relative to the mountain range. On the average, the ratio OXG/FDUB amounts to about 0.5; this value agrees well with corresponding observational data compiled by Lorenz (1967). In the barotropic experiment (U = 10$\frac{m}{s}$ throughout), the ratio is increased to about 1 for both components in the state of quasi-equilibrium (Fig. 17b,c).

3.5 A wind maximum within the boundary layer

As an instructive example of simulated turbulence effects in detail, we present a low-level wind maximum that develops in the course of our moist experiments and displays a characteristic vertical (Fig.18) and horizontal (Fig. 19) structure. To explain this feature, we have to appreciate the downward increasing evaporation of rain that falls in a band coinciding approximately with the C_M-band of Fig. 20. The related stabilization effect above the surface, which is supported by the night phase of the diurnal cycle, results in the complementary pictures of C_M (Fig. 20) and K_M^v in the ABL (Fig. 21). To consider the dynamical aspects in a Lagrangian manner, we make use of the ageostrophic wind components normal (AGN; Fig. 22a) and parallel (AGS; Fig. 22b) to the geostrophic wind vector. The region of strong turbulent friction causes AGN to get large positive values. The kinetic energy thus gained by the air results in a remarkable supergeostrophic speed which produces the wind maximum. Afterwards, the sequence is reversed.

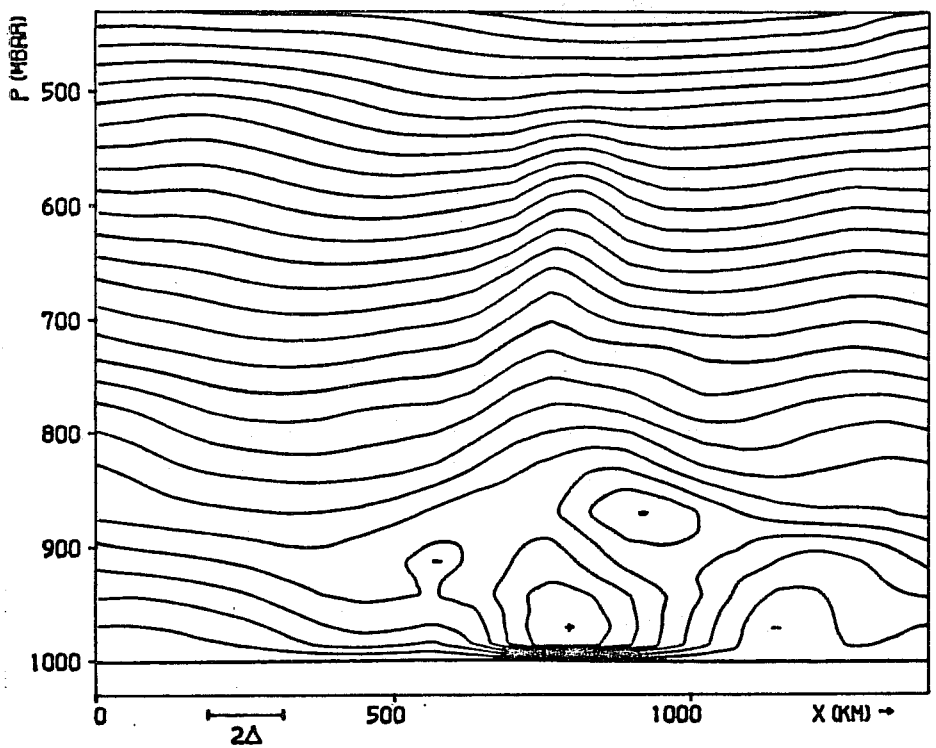

Fig. 18 Wind speed in a (x,z)-cross-section through the channel center (Exp. C17, time 30 h)

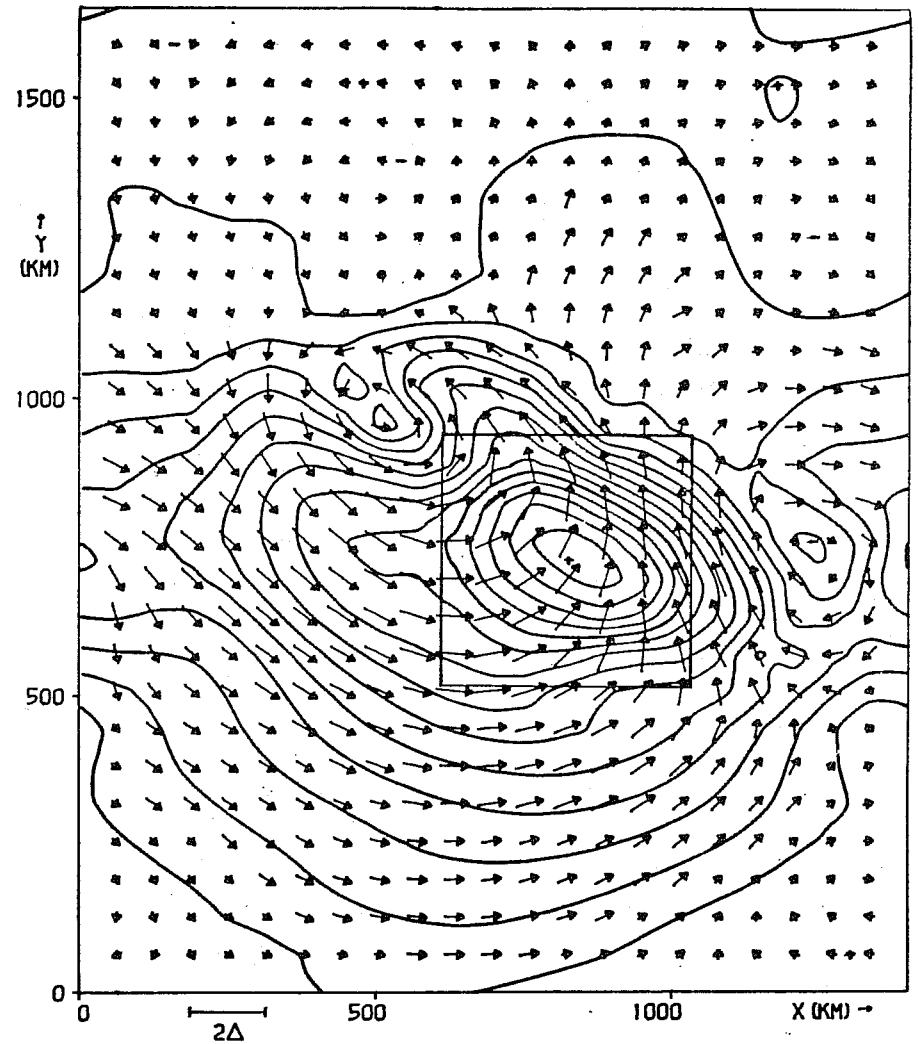

Fig. 19 Wind speed (0.5m s^{-1}) and direction at level σ = 0.92 (Exp. C17 time 30 h)

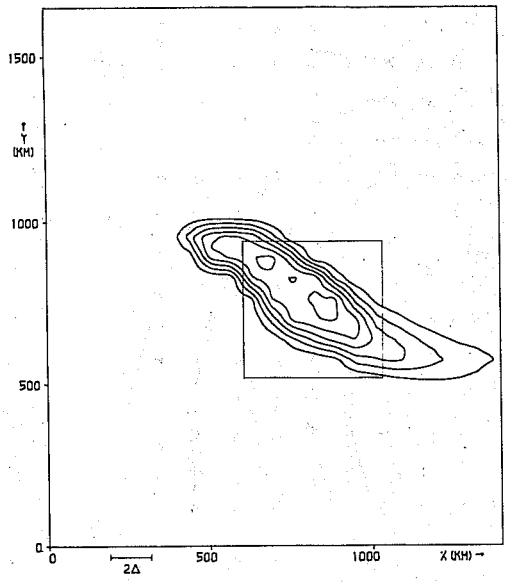

Fig. 20 Turbulent transfer coefficient (0.25 cm s^{-1}) for momentum (Exp. C17, time 30 h)

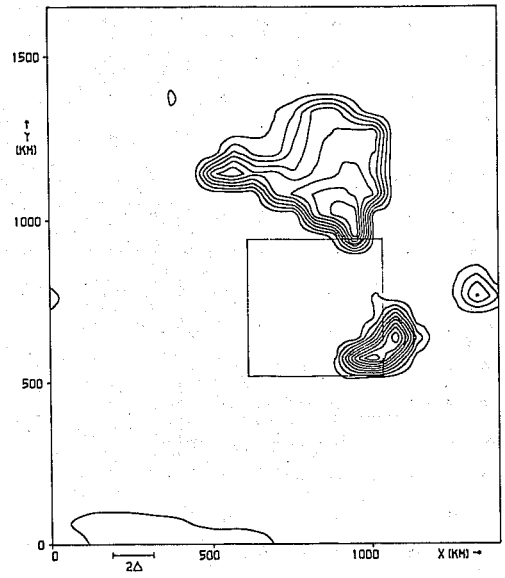

Fig. 21 Turbulent diffusion coefficient (5 m^2 s^{-1}) for momentum at level $\sigma = 0.94$ (Exp. C17, time 30 h)

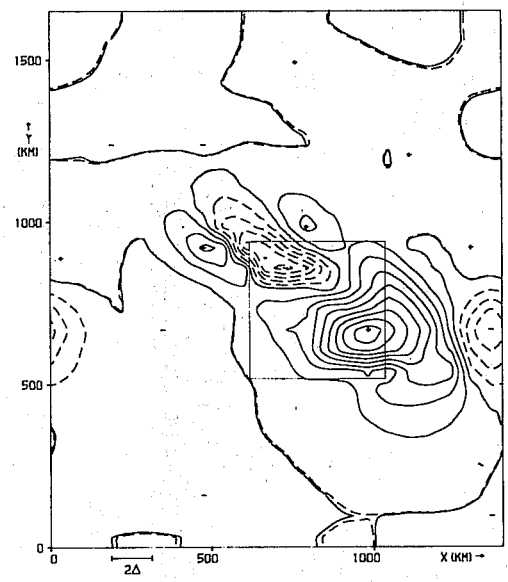

Fig. 22a

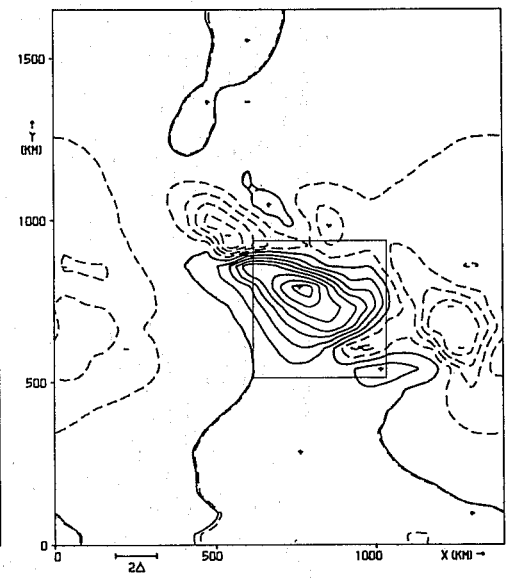

Fig. 22b

Ageostrophic wind components (0.5 m s^{-1}) normal (a) and parallel (b) to the geostrophic wind vector at level $\sigma = 0.92$ (Exp. C17, time 30 h)

4. CONCLUDING REMARKS

The performance of a diagnostic second order closure scheme to parameterize turbulent fluxes in the context of a regional-scale model has been demonstrated - admittedly under the limitations of a channel version. This type of parameterization is considered to represent a kind of upper limit of complexity that is justifiable in an operational weather forecast model. Certainly, this scheme may be gradually elaborated by including equations of a prognostic type. Flux-gradient relations for heat and momentum continue to exist for Level 2.5 (Yamada, 1977) and Level 3 (Yamada and Mellor, 1974 and 1975). But it is questionable if some minor improvements known from 1-dimensional simulations could be incorporated in a numerical system of low vertical resolution.

On the other hand, there are questions of a more fundamental nature. The set of free parameters is generally fixed by means of observations within the Prandtl layer. Does this set hold also for higher layers of the atmosphere? A key position is taken by the characteristic length scale.

The theory has been developped under the assumption of horizontal homogeneity. Are the relations applicable to processes averaged over large areas with underlying complex terrain?

Observational verification is almost non-existent. Hopefully, ALPEX will shed some light on this problem.

5. REFERENCES

Blackadar, A.K. 1962 The vertical distribution of wind and turbulent exchange in a neutral atmosphere. J.Geophys.Res., 67, 3095-3102.

Businger, J.A. 1973 Turbulent transfer in the atmospheric surface layer. In: Haugen, D.A. (Ed.) Workshop on micrometeorology. Boston, Amer.Meteor.Soc., 67-100.

Chen, W.Y. 1974 Energy dissipation rates of free atmospheric turbulence. J.Atmos.Sci., 31, 2222-2225.

Deardorff, J.W. 1973 Three-dimensional numerical modeling of the planetary boundary layer. In: Haugen, D.A. (Ed.) Workshop on micrometeorology. Boston, Amer.Meteor.Soc., 271-311.

Lorenz, E.N. 1967 The nature and theory of the general circulation of the atmosphere. WMO No. 218.TP.115, pp. 161.

Louis, J.-F. 1977 Parameterisation of the surface fluxes. ECMWF Internal Report No. 4, pp. 14.

Louis, J.-F. 1979 A parametric model of vertical eddy fluxes in the atmosphere. Boundary-Layer Meteor., 17, 187-202.

Mellor, G.L. 1973 Analytic prediction of the properties of stratified planetary surface layers. J.Atmos.Sci., 30, 1061-1069.

Mellor, G.L. and Yamada, T. 1974 A hierarchy of turbulence closure models for planetary boundary layers. J.Atmos.Sci., 31, 1791-1806.

Monin, A.S. and Yaglom, A.M. 1971 Statistical fluid mechanics: Mechanics of turbulence. Vol. 1. Cambridge, The MIT Press, pp. 769.

Tiedtke, M.; Geleyn, J.-F.; Hollingsworth, A.; Louis, J.-F. 1979 ECMWF model-parameterization of sub-grid scale processes. ECMWF Technical Report No. 10, pp. 46.

Wieringa, J. 1980 A reevaluation of the Kansas mast influence on measurements of stress and cup anemometer overspeeding. Boundary-Layer Meteor., 18, 411-430.

Working Group on Atmospheric Boundary-Layer Problems 1973 Dynamics of the atmosphere. Atmospheric boundary layer. WMO CAS-VI/Doc. 6, pp. 11.

Yamada, T. 1977 A numerical experiment on pollutant dispersion in a horizontally-homogeneous atmospheric boundary layer. Atmos.Environment, 11, 1015-1024.

Yamada, T. and Mellor, G. 1975 A simulation of the Wangara atmospheric boundary layer data. J.Atmos.Sci., 32, 2309-2329.